Pergamon

Int. J. Solids Structures Vol. 34, No. 15, pp. 1893–1914, 1997

0020–7683/97 $17.00 + .00

PII: S0020–7683(96)00122–9

ON THE EVERSION OF COMPRESSIBLE ELASTIC CYLINDERS

D. M. HAUGHTON and A. ORR
Department of Mathematics, University of Glasgow, University Gardens, Glasgow G12 8QW, Scotland

(*Received* 2 *October* 1995; *in revised form* 20 *June* 1996)

Abstract—We consider the eversion problem for compressible hyperelastic isotropic thick-walled cylinders. We give a new strain–energy function for a highly compressible material that admits an exact solution to the problem with point-wise end conditions. Previously, only averaged loads could be accounted for. Secondly, we investigate the bifurcation problem for a wide range of material models. We find qualitively similar results to those obtained for incompressible materials. While thin-walled cylinders can be everted into other right circular cylinders if the wall-thickness exceeds some critical value, bifurcation into non-cylindrical shapes is possible. © 1997 Elsevier Science Ltd.

1. INTRODUCTION

In a recent paper, Haughton and Orr (1995) considered the basic deformation and bifurcation of everted incompressible elastic cylinders. In particular they found that if a right circular cylinder is thin enough then it can be everted into another right circular cylinder, subjected to zero tractions on the curved surfaces, provided that the ends are subjected to a zero resultant traction. (If zero pointwise tractions are specified on the ends then the ends of the everted cylinder are belled out and exact analytic solutions cannot be obtained.) However, if the cylinder is thicker than some critical value the everted shape will not be cylindrical. The tube undergoes a bifurcation on eversion and will collapse into some non-symmetrical configuration.

The aim of this paper is to investigate the consequences of compressibility. To this end we concentrate largely on the class of Varga materials introduced by Haughton (1987) and independently by Carroll (1988). These strain-energy functions are simple enough to allow significant progress to be made analytically but retain sufficient generality to model a wide range of material behaviour. In particular it is possible to choose parameters that will give incompressible Varga materials at one end of their spectrum and infinitely compressible materials at the other end. The Blatz–Ko (1962) material and one other are considered for comparison.

We start by giving a formulation of the equilibrium equations, assuming that the everted shape will be cylindrical. This basic eversion problem for compressible materials has not received much attention, in contrast to the equivalent problem for incompressible materials, see Rivlin (1949), Chadwick (1972) and Chadwick and Haddon (1972) for example. However, Carroll (1988) has shown, in passing, how the equilibrium equation can be reduced to a quadrature in the case of Harmonic materials. Also, Carroll and Horgan (1990) have obtained an exact solution to the equilibrium equation in the case of a Blatz–Ko material but neither boundary conditions nor end conditions were considered. Here we show that a particular material model allows an exact solution to the eversion problem with pointwise zero tractions applied to the ends of the cylinder. The strain–energy function that allows this solution is highly compressible and could be considered as an alternative to the Blatz–Ko model. For incompressible materials Chadwick (1972), Chadwick and Haddon (1972) and Adeleke (1983) were able to give significant results concerning the existence and uniqueness of the everted shape (within the set of right circular cylinders, non-cylindrical shapes were not considered). Unfortunately, we have not been able to make any general progress on this problem for compressible materials, although computation of

the everted (cylindrical) shape proves to be straightforward for the materials considered and the exact solution obtained is clearly unique.

After a discussion of the basic eversion problem for Varga and Blatz–Ko materials we briefly give a derivation of the incremental equations to look for possible bifurcation modes. The resulting systems of homogeneous equations are solved for critical values of the radius ratio of the cylinder by using the compound matrix method (see Appendix for details). This method has been shown by Haughton and Orr (1995) to be far superior to other methods commonly used in elasticity for bifurcation problems. The bifurcation results are presented graphically to show the effect of other parameters, aspect ratio and compressibility on the different modes of bifurcation. In particular we show that the results for compressible materials are qualitatively similar to those for incompressible materials, see Haughton and Orr (1995), irrespective of the bulk modulus of the material. That is, there exists a critical thickness ratio for a tube of a given material. Thinner tubes may be everted into other right circular cylinders. However, for tubes with a thickness ratio in excess of the critical value a bifurcation into some complicated buckled shape will occur upon eversion and the cylindrical solution (which still exists) will not be seen. For all materials and parameters that we have considered the critical thickness ratio (undeformed inner radius over undeformed outer radius) is always less than 0.55. We find that the aspect ratio of the cylinder is relatively unimportant, all but unrealistically short tubes behave as if they were infinitely long. The post-bifurcation problem to determine the collapsed shape of the cylinder is not considered here.

Finally, we discuss the results in the light of the experimental results on the eversion of tubes give in Truesdell (1978).

2. EVERSION

Suppose that the undeformed compressible isotropic homogeneous elastic tube occupies the region

$$0 < A \leqslant R \leqslant B, \quad 0 \leqslant \Theta \leqslant 2\pi, \quad 0 \leqslant Z \leqslant L, \tag{1}$$

where (R, Θ, Z) are cylindrical polar coordinates. The cylinder is now everted into another right circular cylinder occupying the region

$$0 \leqslant a \leqslant r \leqslant b, \quad 0 \leqslant \theta \leqslant 2\pi, \quad -l \leqslant z \leqslant 0, \tag{2}$$

where (r, θ, z) are also cylindrical polar coordinate and $l > 0$ is a constant. We note that the surface $R = A$ is mapped to the surface $r = b$ and $R = B$ is mapped to $r = a$. The deformation can be described by

$$r = r(R), \quad \theta = \Theta, \quad z = -\lambda Z, \tag{3}$$

where $\lambda > 0$ is a constant such that $l = \lambda L$. The components of the deformation gradient $\mathbf{F}$ referred to cylindrical coordinates are then

$$\mathbf{F} = \begin{bmatrix} \dfrac{\mathrm{d}r}{\mathrm{d}R} & 0 & 0 \\ 0 & \dfrac{r}{R} & 0 \\ 0 & 0 & -\lambda \end{bmatrix}. \tag{4}$$

The principal stretches of this deformation can be written

$$\lambda_r = -\frac{\mathrm{d}r}{\mathrm{d}R}, \quad \lambda_\theta = \frac{r}{R}, \quad \lambda_z = \lambda, \tag{5}$$

where the subscripts denote the appropriate directions. For a compressible material the dilatation J must be positive, and so we can write

$$J = \det(\mathbf{F}) = -\lambda \frac{r}{R}\frac{\mathrm{d}r}{\mathrm{d}R} > 0. \tag{6}$$

The equilibrium equations for the deformation above reduce to the single equation

$$r\frac{\mathrm{d}\sigma_{rr}}{\mathrm{d}r} + \sigma_{rr} - \sigma_{\theta\theta} = 0, \tag{7}$$

where the principal Cauchy stresses σ_{rr}, $\sigma_{\theta\theta}$ and σ_{zz} can be written in terms of the strain-energy function $W = W(\lambda_r, \lambda_\theta, \lambda_z)$ of the material as

$$J\sigma_{ii} = \lambda_i \frac{\partial W}{\partial \lambda_i}, \quad \text{no sum}, \tag{8}$$

where the subscripts i should be regarded as one of (r, θ, z) and we recall that $J = \lambda_r\lambda_\theta\lambda_z$. Ideally we would like to satisfy the point-wise boundary conditions of zero traction on the entire surface of the cylinder,

$$\sigma_{rr}(a, \theta, z) = \sigma_{rr}(b, \theta, z) = 0, \quad 0 \leqslant \theta \leqslant 2\pi, \quad -\lambda L \leqslant z \leqslant 0, \tag{9}$$

and

$$\sigma_{zz}(r, \theta, 0) = \sigma_{zz}(r, \theta, -\lambda L) = 0, \quad 0 \leqslant \theta \leqslant 2\pi, \quad a \leqslant r \leqslant b. \tag{10}$$

However, for most material models the pointwise end conditions (10) are not compatible with the assumed deformation (3). In these cases we follow Rivlin (1949) and all other authors who have considered the eversion of incompressible elastic tubes and reduce our requirement to that of zero resultant load on the ends. We replace (10) with the condition

$$N = 2\pi \int_a^b r\sigma_{zz}\,\mathrm{d}r = 0, \quad z = -\lambda L, 0. \tag{11}$$

Since we have insisted $r = r(R)$, we can change variables in (7) so that the equilibrium equation becomes

$$\frac{\mathrm{d}\sigma_{rr}}{\mathrm{d}R} + \frac{r'}{r}(\sigma_{rr} - \sigma_{\theta\theta}) = 0, \tag{12}$$

where we have written $r' = \mathrm{d}r/\mathrm{d}R$. To solve the problem for $r(R)$ we first guess a value for λ and $b = r(A)$ (say). The boundary condition $(9)_2$ can then be used with (12) and (5) to evaluate the corresponding $r'(A)$. The equilibrium equation (12) can then be treated as an initial value problem for $r(R)$ and hence we obtain $r(B)$ and $r'(B)$. The boundary condition $(9)_1$ is then evaluated and our initial guess for b is modified to ensure that this is satisfied. We then evaluate the end condition (11), our initial guess for λ is modified to ensure that this is satisfied. Hence, (11) and (12) with (5) and (8) are two simultaneous equations for λ and a. These will be evaluated for specific forms of strain-energy functions.

Firstly, we propose a new strain-energy function which allows an exact solution to the basic eversion problem.

2.1. *Exact solution*

Previous investigations of possible everted states have concentrated on incompressible materials and offered only numerical solutions assuming the approximate end conditions (11). Here we are able to solve the eversion problem exactly for a highly compressible material. This has the additional benefit of being a useful check of any numerical techniques employed. Considering the strain-energy function

$$W(\lambda_1, \lambda_2, \lambda_3) = \mu\{(\lambda_1 - 1)^2 + (\lambda_2 - 1)^2 + (\lambda_3 - 1)^2\}, \tag{13}$$

where $\mu > 0$ is the ground state shear modulus, we find that the bulk modulus κ is given by

$$\kappa = \tfrac{2}{3}\mu > 0.$$

Since $\kappa/\mu = 2/3$, we have a very highly compressible material. We note that $\kappa/\mu = 5/3$ for the Blatz–Ko (1962) material and so (13) can be thought of as a homogeneous model for a very soft foam rubber. On substituting (13) into the equilibrium equation (12) with (5) we obtain

$$r'' + \frac{r'}{R} - \frac{r}{R^2} + \frac{2}{R} = 0. \tag{14}$$

Integrating twice produces

$$r(R) = R\frac{c_1}{2} + \frac{c_2}{R} - R\ln R + \frac{R}{2}, \tag{15}$$

where

$$c_1 = \frac{2B^2 \ln B - 2A^2 \ln A}{B^2 - A^2} - 1, \quad c_2 = \frac{A^2 B^2 \ln(B/A)}{B^2 - A^2} \tag{16}$$

are obtainable from the boundary conditions (9). Using (16) and $r(A) = b$, $r(B) = a$ we find

$$a = \frac{2A^2 B \ln(B/A)}{B^2 - A^2}, \quad b = \frac{2AB^2 \ln(B/A)}{B^2 - A^2}, \tag{17}$$

where a, b are the inner and outer deformed radii, respectively. In particular we note that $b/a = B/A$ so that the proportions of the cylinder are maintained. It is a straightforward matter to show that both a/B and b/B are monotonic increasing functions of A/B, hence, as the undeformed shell increases in thickness, so does the overall radius of the everted shell. We now turn our attention to the axial stretch λ to discover the final geometry. For this particular material it is possible to satisfy the original exact eversion problem where we insist that the axial stress is identically zero at each point on the ends of the cylinder. From (13) and (8):

$$\sigma_{zz} = \frac{2\mu\lambda}{J}(\lambda - 1),$$

and so the pointwise end conditions (10) are satisfied for $\lambda = 1$. In passing it should be noted that this is the only solution obtainable from the approximate end conditions. Finally, we note that $a > 0$ for the initial geometry (1) and so the cavity cannot close upon eversion.

2.2. *Varga materials*

We consider the class of Varga materials

$$W(\lambda_1, \lambda_2, \lambda_3) = 2\mu(\lambda_1 + \lambda_2 + \lambda_3 - g(J)), \tag{18}$$

where $\mu > 0$ is the ground state shear modulus of the material and g is an arbitrary function of the dilation J, as defined above.

This strain-energy form is obtained from a general form for compressible materials introduced by Ogden (1972) which is a modified form of the incompressible Varga material where the compressibility is accounted for by the addition of a function g of the dilation J. The explicit form (18) was introduced by Haughton (1987) and independently by Carroll (1988).

The only constraints on the function $g(J)$ are

$$g(1) = 3, \quad g'(1) = 1, \quad g''(1) < -\tfrac{2}{3}. \tag{19}$$

These conditions ensure zero energy and zero stress in the undeformed configuration and a positive bulk modulus respectively.

For explicit calculations we define

$$g(J) = \frac{1 - J^{-\beta}}{\beta} + 3, \quad \beta \neq 0, \tag{20}$$

which satisfies conditions (19) provided $\beta > -\frac{1}{3}$, $\beta \neq 0$. In terms of (18) we can write the bulk modulus as

$$\kappa = 2\mu(\beta + \tfrac{1}{3}). \tag{21}$$

The parameter β then allows us to consider materials with the widest possible range of compressibilities. The incompressible Varga material corresponds to the limit as $\kappa \to \infty$ where we also see $\beta \to \infty$.

Since exact solutions are not available to the equilibrium equations (12) with (9) and (11) we illustrate the behaviour of different tubes graphically. In Fig. 1 we investigate the behaviour of the axial stretch λ as we vary the compressibility of the tube (κ/μ). We can see that λ tends to 1 as β tends to zero for a wide range of initial radii ratio A/B. For this

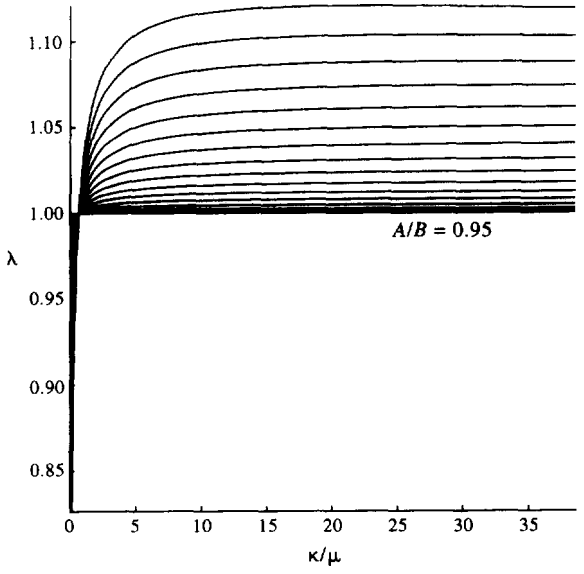

Fig. 1. Plot of axial stretch λ against κ/μ for a variety of initial thicknesses $A/B = 0.2(0.05)0.95$.

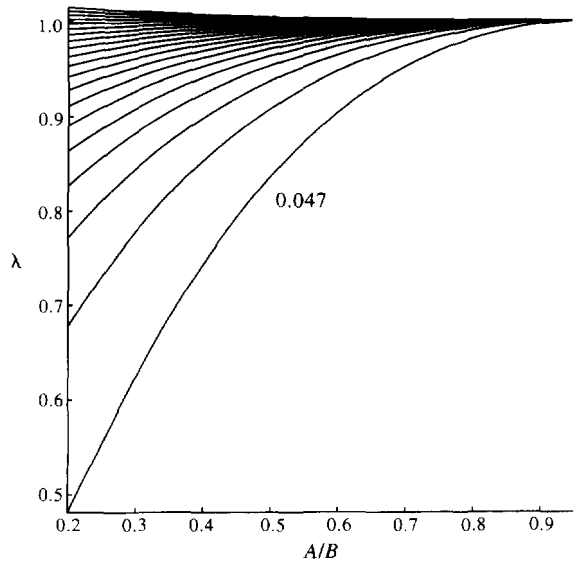

Fig. 2. Plot of axial stretch λ against the undeformed thickness A/B, $\kappa/\mu = 0.047 \ldots 0.81$ ($\beta = -0.31(0.02)0.07$).

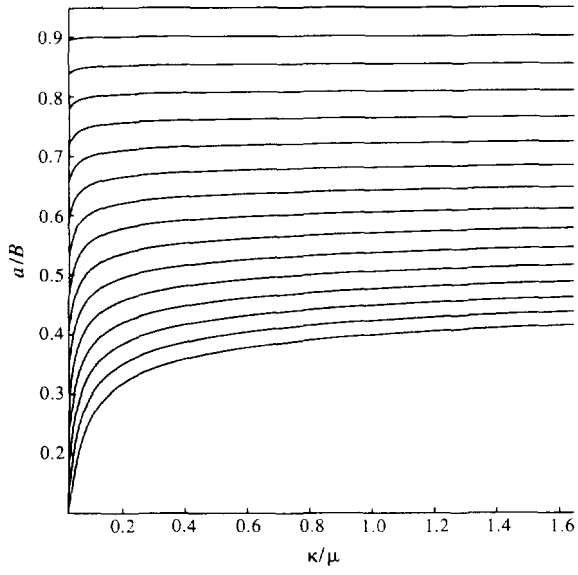

Fig. 3. Plot of deformed inner radius a/B against κ/μ for a variety of initial thicknesses $A/B = 0.2(0.05)0.95$.

value of β we have $\kappa/\mu = 2/3$ which corresponds to a highly compressible cylinder. It is perhaps a coincidence that the exact material (13) has a value $\kappa/\mu = 2/3$ and also gives the solution $\lambda = 1$. We also observe that $\lambda \equiv 1$ for $A/B \to 1$. This limit coincides with the membrane limit. For the extensive range of initial radii ratio plotted we see that provided κ/μ is not close to zero all deformed tubes qualitatively mimic the behaviour of incompressible cylinders. This is the effect anticipated by Truesdell (1978). In Fig. 2 we interchange the roles of initial geometry A/B and compressibility κ/μ to show how the axial stretch λ behaves against the undeformed thickness AB for Varga materials of differing compressibilities.

As we expect from Fig. 1, if $\beta < 0$ then λ increases with decreasing thickness whereas the reverse holds for $\beta > 0$.

We now turn our attention to the deformed inner radius of the everted cylinder. In Fig. 3 we plot the deformed inner radius ratio a/B against κ/μ. In this figure we note that the deformed inner radius $a > A$ unless $\kappa/\mu \ll 1$. Physically we interpret this as the inner hole of the cylinder expanding for all but very highly compressible materials.

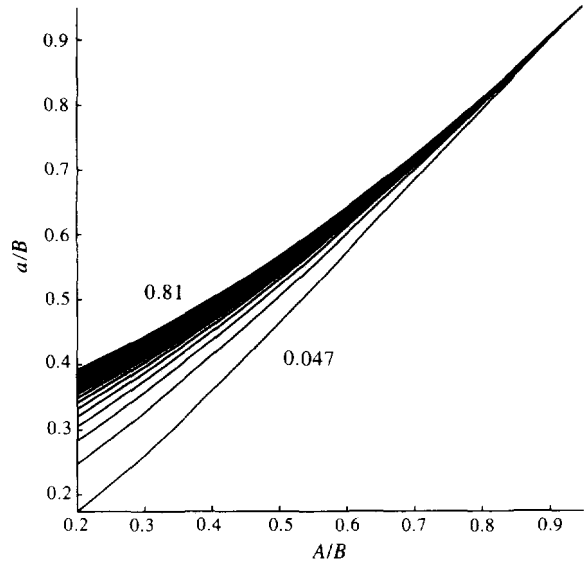

Fig. 4. Plot of deformed inner radius a/B against initial thickness A/B for highly compressive materials. $\kappa/\mu = 0.047 \ldots 0.81$.

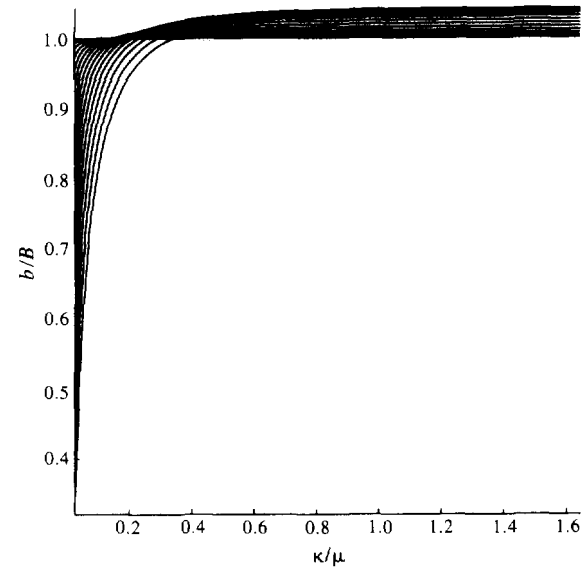

Fig. 5. Plot of the deformed outer radius b/B against κ/μ for a wide range of initial thicknesses $A/B = 0.2(0.05)0.95$.

In Fig. 4 we see that the deformed inner radius ratio a/B is monotonic increasing with the undeformed radius A/B for highly compressible Varga materials. This is in keeping with the results for the exact solution (15) with (16) and (17). However, we see in Fig. 5 that this is not necessarily the case for the deformed outer radius b/B. If we fix the value of κ/μ the outer radius may have a local maximum when regarded as a function of the undeformed thickness A/B as shown in Fig. 6. It is also demonstrated that the local maximum of b/B depends on the compressibility of the material. As the material becomes more compressible the local maximum disappears.

We now consider the non-dimensionalised stresses in the cylinder. In Fig. 7 we plot the three principal stresses for $\kappa/\mu = 7/6$ ($\beta = 0.25$) for an initial thickness $A/B = 0.25$. Qualitatively we note that the stresses are similar to those observed for incompressible materials, [1, Fig. 3] for example. We observe that $\sigma_{rr} \leqslant 0$ throughout the tube and is zero on the ends of the cylinder as required by the boundary conditions (9). Also, the hoop stress $\sigma_{\theta\theta}$ reflects the fact that the tube will have the inner undeformed surface stretched and the outer undeformed surface will undergo compression. It is known that the eversions

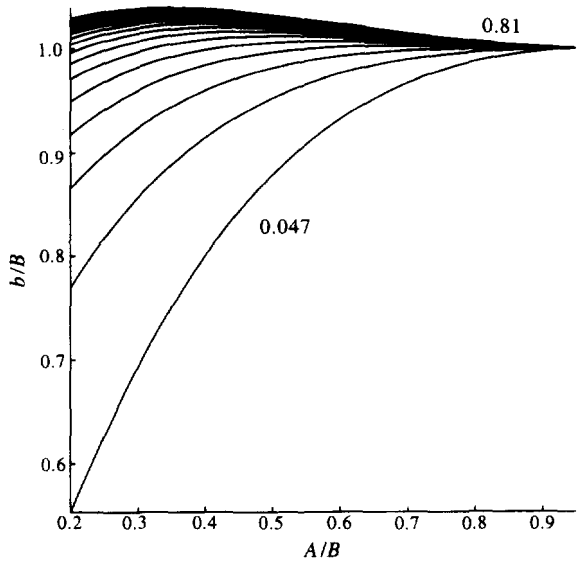

Fig. 6. Plot of the deformed outer radius b/B against the initial thickness A/B for $\kappa/\mu = 0.047 \ldots 0.81$.

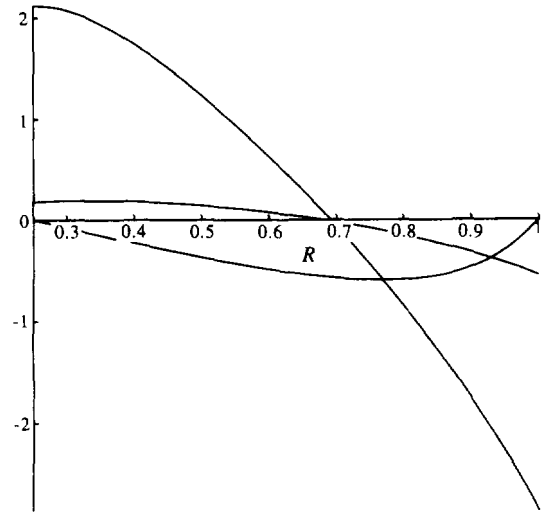

Fig. 7. Plot of the non-dimensional stresses $\sigma_{\theta\theta}/\mu$, σ_{zz}/μ, σ_{rr}/μ, against the undeformed radius R for a tube with $A/B = 0.25$, $\beta = 0.25$ ($\kappa/\mu = 7/6$). For $R = 0.25$, $\sigma_{\theta\theta}/\mu$ is the upper curve, σ_{zz}/μ the middle curve and $\sigma_{rr}(0.25)/\mu = 0$.

of actual tubes with zero applied traction have "belled" ends. We have assumed that the deformation is of the form (3) and consequently have to apply the approximate end condition (11). This effectively removes this belling from the ends. The axial loading required to do this is also shown in Fig. 7. In particular we note that the undeformed inner portion of the shell is subjected to an axial tension and the undeformed outer portion to an axial compression.

From Fig. 1 we can see that as β moves through zero the nature of the deformation is changed. We therefore consider, in Fig. 8, the stresses for the same initial thickness $A/B = 0.25$ but with $\kappa/\mu = 1/6$ ($\beta = -0.25$). As can be seen from Figs 7 and 8 the main difference in the stresses is in the change in sign of the axial stress σ_{zz}. This change in the behaviour of the stress is consistent with the axial stretch changing from $\lambda > 1$ to $\lambda < 1$ as β moves through zero. Since the deformation undergoes a qualitative change as β passes through zero we study the case $\beta \to 0$ analytically. In this limiting case the equilibrium equation (12) reduces to

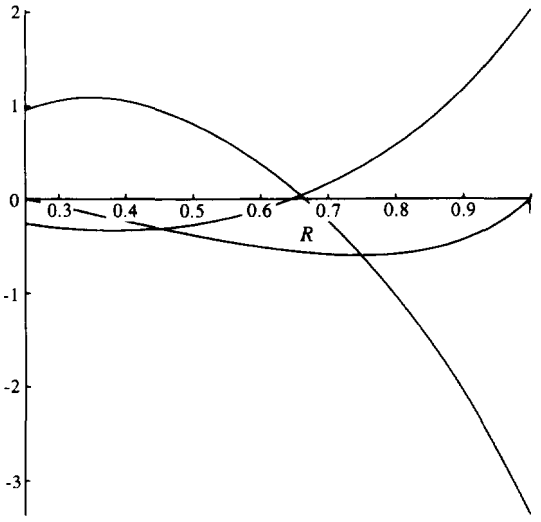

Fig. 8. Plots of the non-dimensionalised stresses $\sigma_{\theta\theta}/\mu$, σ_{zz}/μ, σ_{rr}/μ, against the undeformed radius R for a tube with $A/B = 0.25$, $\beta = -0.25$ ($\kappa/\mu = 1/6$). For $R = 0.25$ $\sigma_{\theta\theta}/\mu$ is the upper curve, σ_{zz}/μ the lower curve and $\sigma_{rr}(0.25)/\mu = 0$.

$$r'' - \frac{r'}{R} + (r')^2\left(\frac{1}{r} - \frac{2}{R}\right) = 0. \tag{22}$$

As pointed out by Hill (1993), the transformation

$$R = \mathrm{e}^t, \quad u = r/R, \quad p = \frac{\mathrm{d}u}{\mathrm{d}t},$$

will always reduce any cylindrical or spherical equilibrium equation to first order, irrespective of the material model. Applying this transformation to (22) we have

$$p\left\{\frac{\mathrm{d}p}{\mathrm{d}u} + p\left(\frac{1}{u} - 2\right) + 2(1-2u)\right\} = 2u^2.$$

Unfortunately we have not been able to solve this analytically. If we look at the radial boundary conditions (9) we obtain

$$\frac{2\mu B}{\lambda a}\left(1 + \frac{1}{r'(B)}\right) = 0,$$

and hence

$$r'(B) \to -1, \quad \text{as } \beta \to 0$$

similarly we find $r'(A) \to -1$, and the axial load N we have

$$-\frac{2\mu}{\lambda}(1 - 1/\lambda)\int_A^B r\,\mathrm{d}R = 0,$$

thus, since $r(R) > 0$, we conclude $\lambda = 1$ and from (8) $\sigma_{zz} \equiv 0$. We are therefore able to solve the pointwise boundary conditions for the material (18) with (20) in the limit as β tends to zero.

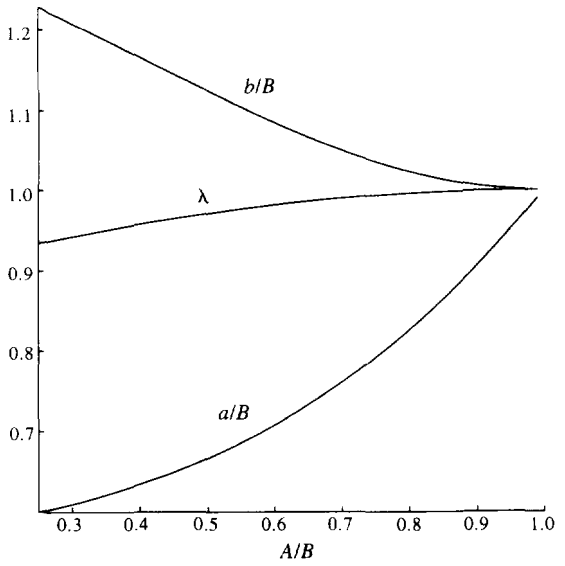

Fig. 9. Plot of the deformed outer radius b/B (upper curve), the axial stretch λ (middle curve) and the deformed inner radius a/B against the initial thickness A/B for the Blatz–Ko material.

2.3. *Blatz–Ko material*

Blatz and Ko (1962) proposed the strain-energy

$$W = \frac{\mu}{2}(\lambda_1^{-2} + \lambda_2^{\ 2} + \lambda_3^{-2} + 2\lambda_1\lambda_2\lambda_3 - 5), \tag{23}$$

where $\mu > 0$ is the ground state shear modulus, based on experiments on foamed polyurethane rubber. We find

$$\kappa/\mu = 5/3.$$

Before presenting any numerical results we first note that the eversion of cylindrical tubes composed of Blatz–Ko material has received some formal attention. Carroll and Horgan (1990) following the earlier work of Chung *et al.* (1986) on (non-eversion) cylindrical problems, provide a rather complicated closed form parametric solution to the problem. However, no boundary condition nor end conditions were considered.

In Fig. 9 we plot three curves for the axial stretch λ, the deformed outer radius b and the deformed inner radius a for various initial geometries. We see that for all undeformed thickness ratios A/B the axial stretch $\lambda < 1$ with λ monotonic increasing in A/B. We can also see that as $A \to B$ then $\lambda \to 1$ and $a \to b$ as we would expect for a membrane cylinder. From Fig. 9 we observe that b/B is monotonic decreasing and for a thick cylinder with $A/B = 0.25$, say, we find $\lambda_\theta(b) \approx 5$ which represents a large tensile stretch and $\lambda_\theta(a) \approx 0.6$ which is a large compressive stretch. We find that the deformed radius a/B is monotonic increasing in A/B. Comparing with Figs 1–6 for Varga materials with a similar bulk modulus we see that the axial stretch and both deformed radii tend to be larger for the Blatz–Ko material.

3. THE INCREMENTAL EQUATIONS

For full details and derivation of equations, Haughton and Ogden (1979a) should be consulted. See also Haughton and Orr (1995) for details applying to the eversion of incompressible materials. In the absence of body forces the incremental equilibrium equations can be written

$$\operatorname{div} \dot{\mathbf{s}}_0 = \mathbf{0}, \tag{24}$$

where div is the divergence operator in the current configuration and $\dot{\mathbf{s}}_0$ is the increment in the nominal stress referred to the current configuration. Henceforth $\dot{\mathbf{x}}$ will denote an increment in the quantity $\mathbf{x}$ and the subscript zero will denote evaluation in the current configuration. Since no extra loading is imposed on the surface of the body the incremental boundary conditions are given by

$$\dot{\mathbf{s}}_0^T \mathbf{N} = 0, \tag{25}$$

where $\mathbf{N}$ is a unit outward normal in the reference configuration. The incremental constitutive law can be written

$$\dot{\mathbf{s}}_0 = \mathbf{B}\boldsymbol{\eta}^T, \tag{26}$$

where $\mathbf{B}$ is the fourth order tensor of instantaneous moduli in the current configuration, $\mathbf{I}$ is the identity and we have $\boldsymbol{\eta}$ for $\dot{\mathbf{F}}_0$. The non-zero components of $\mathbf{B}$ are

$$\left.\begin{aligned} B_{ijij} &= \lambda_i^2 \frac{\sigma_{ii} - \sigma_{jj}}{\lambda_i^2 - \lambda_j^2}, \quad \lambda_i \neq \lambda_j, \\ JB_{iijj} &= JB_{jjii} = \lambda_i \lambda_j \frac{\partial^2 W}{\partial \lambda_i \partial \lambda_j}, \\ B_{ijij} - B_{ijji} &= B_{ijij} - B_{jiij} = \sigma_{ii}, \quad i \neq j. \end{aligned}\right\} \tag{27}$$

where J is the dilatation. Using cylindrical based vectors $\mathbf{e}_1$, $\mathbf{e}_2$, $\mathbf{e}_3$ where the $(1, 2, 3)$ directions correspond to (θ, z, r), respectively, (24) is expressed as

$$\dot{s}_{0ji,j} - \dot{s}_{0jl}\mathbf{e}_k \cdot \mathbf{e}_{j,k} + \dot{s}_{0kj}\mathbf{e}_i \cdot \mathbf{e}_{j,k} = 0, \quad (i = 1, 2, 3), \tag{28}$$

where the non-zero values of $\mathbf{e}_i \cdot \mathbf{e}_{j,k}$ for cylindrical coordinates can be obtained from Haughton and Ogden (1979b).

We write

$$\dot{\mathbf{x}}_0 = v(r, \theta, z)\mathbf{e}_1 + w(r, \theta, z)\mathbf{e}_2 + u(r, \theta, z)\mathbf{e}_3. \tag{29}$$

Hence $\boldsymbol{\eta}$ has components

$$\boldsymbol{\eta} = \begin{bmatrix} (u + v_\theta)/r & v_z & v_r \\ w_\theta/r & w_z & w_r \\ (u_\theta - v)/r & u_z & u_r \end{bmatrix}, \tag{30}$$

in cylindrical coordinates where (θ, z, r) subscripts denote partial derivatives. Substituting (26) with (30) into (28) we obtain

$$\begin{aligned} &B_{2323}u_{zz} + (B_{2332} + B_{2233})w_{zr} + (B_{1331} + B_{1133})\frac{v_{r\theta}}{r} + (rB'_{1133} - B_{1313} - B_{1111})\frac{v_\theta}{r^2} + B_{3333}u_{rr} \\ &+ (rB'_{3333} + B_{3333})\frac{u_r}{r} + (rB'_{1133} - B_{1111})\frac{u}{r^2} + (rB'_{2233} - B_{1122} + B_{2233})\frac{w_z}{r} + B_{1313}\frac{u_{\theta\theta}}{r^2} = 0, \end{aligned} \tag{31}$$

$$(rB'_{3223}+B_{1122}+B_{3223})\frac{u_z}{r}+(rB'_{3232}+B_{3232})\frac{w_r}{r}+(B_{2233}+B_{3223})u_{rz}+(B_{1122}+B_{1221})\frac{v_{z\theta}}{r}$$
$$+B_{1212}\frac{w_{\theta\theta}}{r^2}+B_{2222}w_{zz}+B_{3232}w_{rr}=0, \quad (32)$$

$$+\left(B_{1122}+B_{3131}v_{rr}+B_{1111}\frac{v_{\theta\theta}}{r^2}+B_{2121}v_{zz}+B_{2112}\right)\frac{w_{\theta z}}{r}+(rB'_{3131}+B_{3131})\frac{v_r}{r}$$
$$+(B_{1111}+rB'_{3113}+B_{1313})\frac{u_\theta}{r^2}-(rB'_{3113}+B_{1313})\frac{v}{r^2}+(B_{1133}+B_{3113})\frac{u_{r\theta}}{r}=0, \quad (33)$$

where $(')$ denotes differentiation with respect to r. We shall solve these equations by setting

$$u=f(r)\cos m\theta\cos\alpha z,$$
$$v=g(r)\sin m\theta\cos\alpha z,$$
$$w=h(r)\cos m\theta\sin\alpha z, \quad (34)$$

where we assume the incremental displacement variables are single valued with the mode number m an integer greater than zero. We interpret the parameter α by insisting that we have zero incremental end displacement w which gives

$$\alpha=n\pi/l, \quad n=1,2,3,\ldots. \quad (35)$$

Since the axial mode number n and the length $L(=\lambda l)$ appear only in the combination n/L, we shall regard n as being fixed at unity so that α is inversely proportional to the length of the tube. Substituting (34) into (31)–(33) produces, respectively,

$$(rB'_{3333}+B_{3333})f'/r+(rB'_{1133}-B_{1313}-B_{1111})mg/r^2$$
$$+(B_{1331}+B_{1133})mg'/r-(rB'_{2233}-B_{1122}+B_{2233})\alpha h/r$$
$$+(rB'_{1133}-B_{1111}-m^2B_{1313}-\alpha^2r^2B_{2323})f/r^2-(B_{2332}+B_{2233})\alpha h'+B_{3333}f''=0, \quad (36)$$

$$(rB_{3223}+B_{1122}+B_{3223})\alpha f/r+(B_{2233}+B_{3223})\alpha f'+(B_{1122}+B_{1221})\alpha mg/r$$
$$-(m^2B_{1212}-\alpha^2r^2B_{2222})h/r^2+(rB'_{3232}+B_{3232})h'/r+B_{3232}h''=0, \quad (37)$$

$$(B_{1111}+rB'_{3113}+B_{1313})mf/r^2+(B_{1133}+B_{3113})mf'/r-(rB'_{3131}+B_{3131})g'/r$$
$$-B_{3131}g''-(B_{1122}+B_{2112})m\alpha h/r+(m^2B_{1111}+rB'_{3113}+B_{1313}+\alpha^2r^2B_{2121})g/r^2=0. \quad (38)$$

The corresponding boundary conditions (25) on the curved surfaces becomes

$$\left.\begin{aligned} rg'-g-mf&=0,\\ \alpha f+h&=0,\\ B_{1133}(1-m^2)f/r+B_{3333}f'+mB_{1133}g'-\alpha B_{2233}h&=0,\end{aligned}\right\} r=a,b. \quad (39)$$

4. COMPRESSIBLE BIFURCATION RESULTS

As for incompressible materials, Haughton and Orr (1995), we find that the mode number $m=1$ does not give any bifurcation points and so we confine our attention to $m\geqslant 2$. Firstly we consider the class of Varga materials (23). We begin by studying the

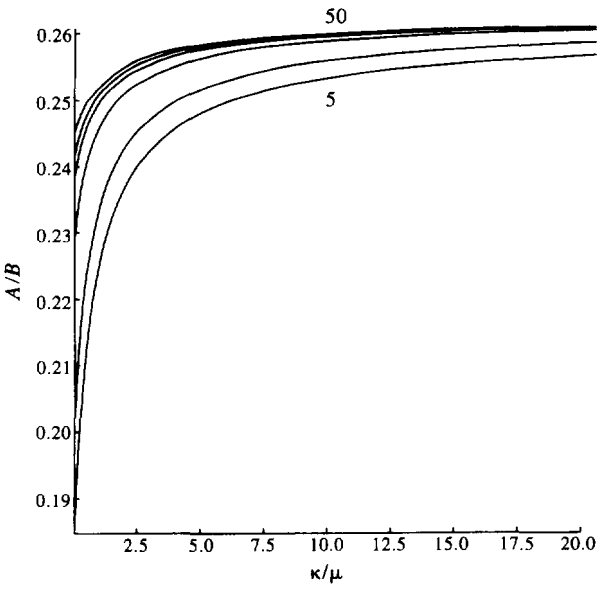

Fig. 10. Plot of the critical values of A/B vs κ/μ for the compressible Varga material for mode $m = 2$. $L/B = 5, 6, 10, 15, 20, 50$.

effects of varying the length of the cylinder on the critical thickness A/B. In Fig. 10 we plot the critical values of A/B against the compressibility κ/μ of the material for various length to radius ratio L/B. We fix the mode number m to be 2. Immediately it can be seen that as we increase L/B the critical thickness A/B increases and the bifurcation curves appear to converge to some limiting curve of critical thickness. We note that although the curves converge to a limit we do not encounter any points of intersection between distinct curves. Considering the case $L/B \to \infty$ analytically for a general material, which in terms of the incremental deformation (34), is equivalent to $\alpha \to 0$, we find that the incremental equations simplify and the equation for h decouples. Unfortunately, no analytical solution is forthcoming.

Returning to Fig. 10 we observe that as κ/μ increases, and hence the material tends towards the incompressible limit, the bunching effect is more evident. For small values of κ/μ, and hence more compressible materials, we observe that the critical thickness A/B obtained has a greater dependence on the initial length to radius ratio L/B of the undeformed tube. We can therefore say that the more compressible a material the greater the length to radius ratio L/B must be before we may consider it as being effectively infinitely long. This graph seems to suggest that for a particular value of L/B the critical thickness A/B obtained is directly proportional κ/μ and hence to the compressibility of the material.

We can readily see that for $\kappa/\mu > 10$ the critical thickness A/B is relatively constant for shorter cylinders. This corresponds to the results on incompressible materials by Haughton and Orr (1995), where it was shown that for $L/B > 5$ (approximately) the cylinder behaves as if it were infinitely long. For actual short highly compressible tubes we may expect that both the compressibility and the end effects will affect the value of the critical thickness A/B obtained as a higher proportion of the deformed tube will be non-cylindrical.

Using the above results as our motivation we now examine the effects that the compressibility of the material has on the critical thickness A/B obtained upon bifurcation. We achieve this by varying the parameter β which is connect to κ/μ by (26). As before we plot κ/μ to add physical meaning to any results obtained. In Fig. 11 we plot the critical thickness A/B against the compressibility factor κ/μ for a wide variety of mode numbers. The most noticeable feature of the graphs is that for $\kappa/\mu > 5$ the critical thickness A/B appears to be virtually constant for any given mode number. We can also see that as we increase the mode number m the critical thickness A/B increases and the curves converge to some asymptotic value. This suggests that the higher mode numbers, and in particular the infinite mode ($m \to \infty$), will be the most important as they produce the thinnest bifurcated shells. If we consider the infinite mode analytically, we simply find that $\dot{\mathbf{x}} = 0$. We therefore

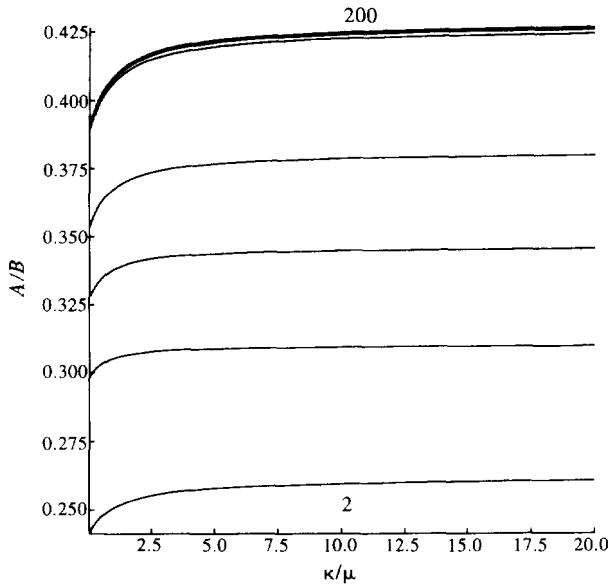

Fig. 11. Plot of the critical values of A/B vs κ/μ for the compressible Varga material. Mode numbers $m = 2, 4, 8, 10, 100, 150, 200$, $L/B = 20$.

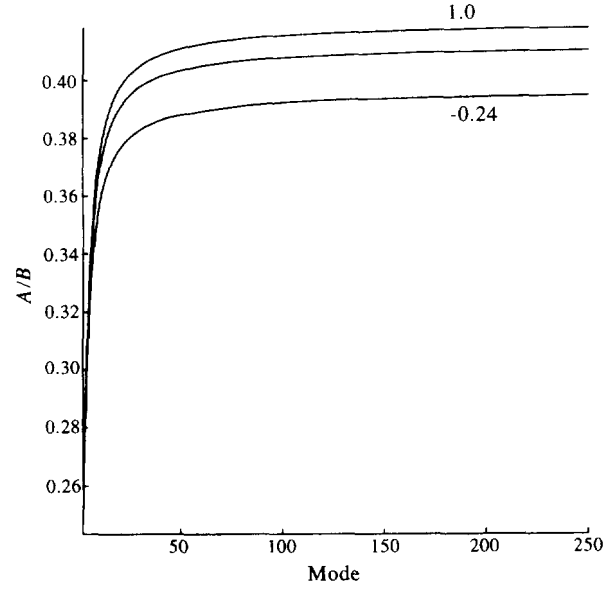

Fig. 12. Plot of the critical values of A/B vs m for the compressible Varga material for $L/B = 20$, $\beta = -0.24, 0.24, 1.0$.

conclude that the infinite mode is not attainable numerically. From Figs 10 and 11 we note that the critical value of A/B tends to increase with κ/μ. This would seem to indicate that compressible cylinders are less likely to undergo bifurcation on eversion. In Fig. 11 we see that it is only for $\kappa/\mu < 5/2$, which corresponds to $\beta < 1$, where we see any appreciable change in the critical thickness. Here we find that the critical thickness A/B decreases as the material becomes highly compressive. Figure 11 demonstrates that the main area of interest in our bifurcation curves is for $\kappa/\mu < 2/3$, which corresponds to $\beta < 0$, and to highly compressible material forms. We now study this area in more detail.

In Fig. 12 we plot the critical thickness A/B against the mode number m. Here we vary the compressibility factor κ/μ and consider three compressible Varga forms which correspond to both $\beta < 0$ and $\beta > 0$. The data for the mode number m is in fact a discrete set of points and have been joined up for ease of presentation.

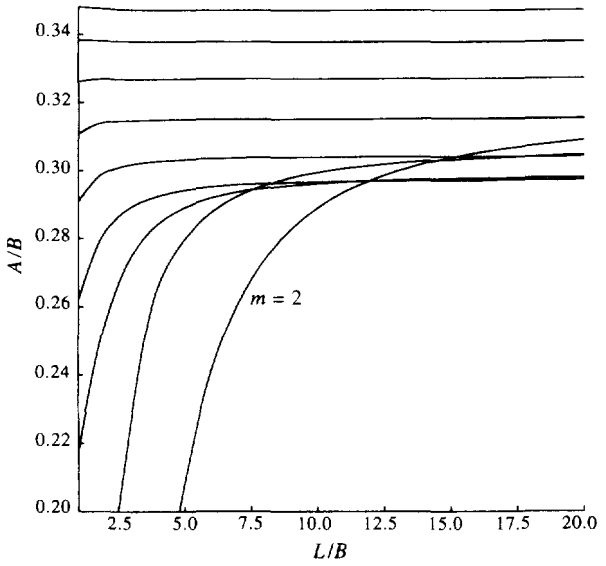

Fig. 13. Plot of the critical values of A/B vs L/B for the Blatz–Ko material. Mode numbers $m = 2$, 3, 4, 5, 6, 7, 8, 9, 10.

For comparison, we now consider the Blatz–Ko strain-energy form (23). This material has $\kappa/\mu = 5/3$ and is therefore highly compressible. We may therefore expect to be able to draw comparisons between the bifurcation of Blatz–Ko materials and highly compressible Varga materials.

In Fig. 13 we plot the critical cylinder thickness A/B against the length to radius ratio L/B of the cylinder for a range of mode numbers. We can clearly see from Fig. 13 that the length only effects the lower mode numbers significantly. For $m \geqslant 6$ we find that, for $L/B > 5$, the cylinder behaves as an infinite one. Indeed, for $m \geqslant$ g we observe that the critical radius produced with a short cylinder with $L/B = 2$ is indistinguishable from the critical radius produced by an infinitely long cylinder. For the lower mode numbers ($m \leqslant 5$) we see that as we decrease the length of the tube the critical radius at which the tube bifurcates decreases dramatically. However, this is not important as for very short highly compressible tubes we would expect the end effects to play a significant role. We also observe that, as m increases, the critical radius A also increases and thus we would expect the higher order ($m \to \infty$) mode numbers to be the most important. We are therefore able to consider all tubes to be effectively infinitely long.

Another point of interest is the non-monotonic increasing relationship between the mode number m and the critical thickness A/B. However, A/B is monotonic increasing in L/B for a particular mode number m. We observe that the lower mode numbers ($m = 2, 3$) intersect several of the higher order mode number curves. This behaviour was not evident in the bifurcation of the highly compressible Varga forms where we found no intersection of curves. Although we may expect similar behaviour due to the comparable compressibilities of the materials it must be stressed that both materials are governed by different strain–energy functions and that it is these functions that determine the bifurcation criteria.

In Fig. 14 we focus our attention on the relationship between the critical radius A/B and the mode number m. Here we consider a Blatz–Ko tube with $L/B = 20$. The first thing we note is the existence of multiple bifurcation points for any given mode number. It should however be noted that this is a discrete set of points and that the lines are just to give a representation of the data. We hence place no importance on the anomalous line. From the graph it is clear that as we increase m, more bifurcation points are produced and the value of the critical radius increases. We would expect the uppermost curve to be the most important since all tubes thicker than this will be unstable. The minimum turning point on the upper curve is explained by consulting the previous figure where we see that for small mode numbers the bifurcation curves cross each other.

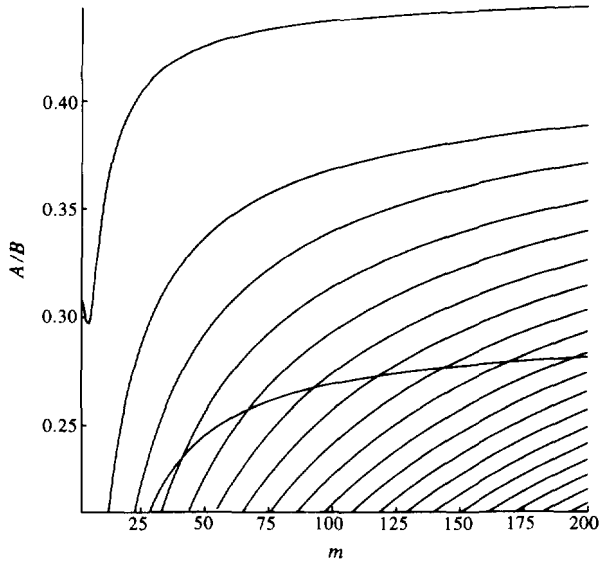

Fig. 14. Plot of the critical values of A/B vs the mode number m for the Blatz–Ko material $L/B = 20$.

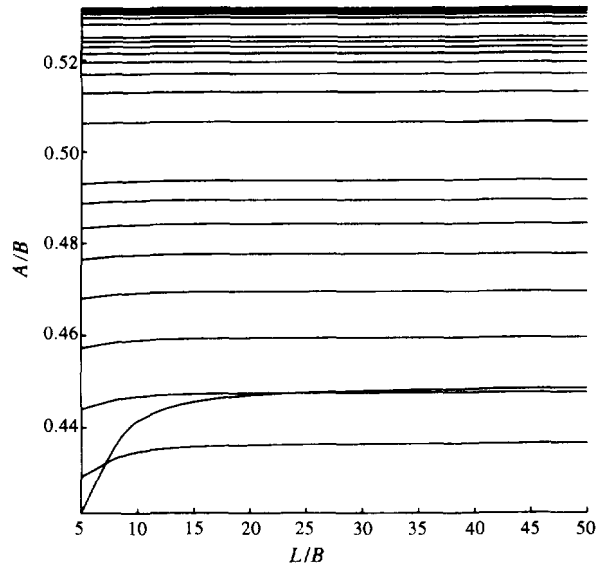

Fig. 15. Plot of the critical values of A/B vs L/B for the Exact Solution material. Mode numbers $m = 2(1)10, 15(5)50, 100(25)200$.

Finally, the "exact" material is defined in (13) and has $\kappa/\mu = 2/3$. As before we will compare the bifurcation results to those obtained for other highly compressible forms. Here we first consider the effect of the length to radius ratio on the bifurcation modes produced. In Fig. 15 we plot the critical thickness A/B against the length to radius ratio L/B for a selection of mode numbers m.

The uppermost curve corresponds to $m = 200$. We can see that the critical value of A/B is then monotonic decreasing with the mode number m until $m = 5$. For low mode numbers ($m < 4$) we see that the picture is not clear. Considering $m = 2$ we see that as the cylinder becomes longer the critical initial thickness at which the tube bifurcates appears to be monotonic increasing. In the case of $m = 3$, we see that for $L/B > 10$ the cylinder can be regarded as infinite. These small mode numbers produce results which are similar to the Blatz–Ko material, see Fig. 13. As we increase m ($m > 5$) we see that for $L/B > 5$ the cylinder behaves as an infinite one. This result ties in with the results for incompressible materials. Again we would expect end effects to play an important role in cylinders with

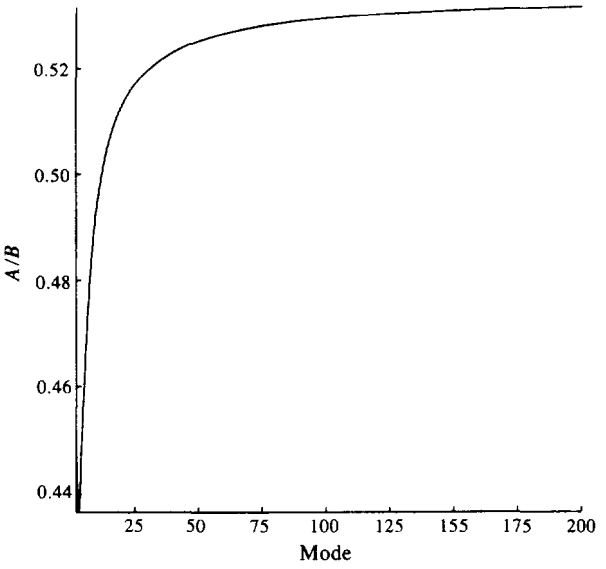

Fig. 16. Plot of the critical values of A/B vs m for the Blatz–Ko material. $L/B = 50$.

$L/B < 5$. We also observe that as the mode number m is increased the critical thickness, A/B is monotonic increasing with no maximum occurring for $m < 200$. This is not too surprising as the incompressible Varga material does not attain a local maximum until $m = 200{,}000$. Unfortunately we are not able to consider $m > 200$ for the "exact" material as the numerical method breaks down. The numerical method, as described in the Appendix, requires some complicated function of the material model, deformation and incremental displacement $\dot{\mathbf{x}}_0$ to be zero. However, as mentioned above, the limiting case $m \to \infty$ gives only the trivial solution $\dot{\mathbf{x}}_0 = 0$ and so, in the limit as $m \to \infty$, the numerical method will predict bifurcation points everywhere. As m gets "large" the numerical method unavoidably starts to give spurious results. We only present results here that are far removed from this problem.

In Fig. 16 we shown how the critical thickness behaves as a function of the mode number m. Here we plot only the uppermost values of A/B for any given mode number. We consider a length to radius ratio of $L/B = 50$, which is effectively infinite. This is comparable to the uppermost curve in Fig. 14 for the Blatz–Ko material. There is a sharp spike (near the origin in Fig. 16) corresponding to the mode $m = 2$ bifurcation curve crossing the mode $m = 3$ bifurcation curve as shown in Fig. 15. This is also consistent with the low mode numbers for the Blatz–Ko material. We can also see that A/B is monotonic increasing in m and appears to be bounded above.

From Fig. 16 we can say that the maximum critical thickness $A/B < 0.550$. On inspection of Fig. 12 we see that as $m \to \infty$ the maximum critical value of $A/B \approx 0.425$ for the compressible Varga material. From the uppermost curve in Fig. 14 we find that the maximum critical thickness for the Blatz–Ko material is approximately $A/B \approx 0.430$.

Since the exact solution material has the greatest value of critical thickness it will undergo a spontaneous bifurcation for the thinnest shells. We also find the compressible Varga material has the thickest initial geometry before it experiences any bifurcation modes. If we consider the compressibilities of the three material classes we do not obtain any correlation between the compressibility of the material and the cylinder thickness necessary to produce bifurcation. As discussed before, we are interested in the upper-most bifurcation curves because they produce the greatest values of the critical thickness A/B. The compressible Varga material has a very wide range of possible compressibilities and supports the eversion of the thickest shells before we reach a bifurcation point. This holds for any value of κ/μ and hence any compressibility. We expect that any cylinder thicker than these values will undergo bifurcation upon eversion. We find that the exact solution material will produce bifurcation modes for the thinnest cylinders. It may be significant that this material

solves the theoretical problem exactly and does not require any loads to satisfy the end conditions.

5. CONCLUSIONS

We have shown that compressible elastic cylinders may undergo a spontaneous bifurcation into a non-cylindrical shape upon being everted. The qualitative results show that, for this problem, compressible cylinders behave in the same way as incompressible cylinders, except for the very highly compressible materials where there are some qualitative differences in the basic deformation of the shell. However, even for very compressible materials the critical radius ratio for the existence of bifurcation remains low. We have also shown that there is a very rapid transition from very short cylinders to those that are effectively infinitely long, in effect all cylinders with a aspect ratio $L/B \geqslant 5$ can be regarded as infinitely long. This suggests that only reasonably thick-walled cylinders ($A/B \leqslant 0.5$) will lose the cylindrical shape on being everted. This is in contrast to the experimental result reported by Truesdell (1978) where a foam rubber cylinder with radius ratio $A/B = 5/6$ underwent a bifurcation upon eversion.

To explain this apparent discrepancy we must investigate the differences between the theoretical analysis given in the paper and the experimental result. Firstly, the theoretical eversion problem uses approximate end conditions to simplify the analysis which will obviously introduce some error. However, we do have some evidence to suggest that this is not a significant error. In Section 2.1 we have found a material model (13) that allows an exact solution to the basic eversion problem, we can also say the same of the Varga material as $\beta \to 0$.

These materials are highly compressible and so we might expect them to provide a reasonable model for the material used by Truesdell (1978). However, when we consider the bifurcation problem for the exact material we find that the critical radius ratio still bears no comparison with the cylinder used by Truesdell (1978), see Fig. 16, although it is interesting to note that the critical radius ratio for this material is higher than that of other equally compressible materials that satisfy only the approximate end conditions.

If, for a moment, we consider thick-walled (incompressible) elastic cylinders subjected to an external pressure we know that only a very modest change in outer radius is required before the cylinder collapses, Haughton and Ogden (1979b), Table 1, for example. It seems likely that we need to reduce the everted outer radius of the cylinder to induce the required bifurcation for thinner walled cylinders; this point is also illustrated in Haughton and Orr (1995), Fig. 1. We have conducted our own very limited experiments on a thick-walled elastic foam paint roller ($A/B = 0.27$). On everting the cylinder there were several interesting features. The belled ends were very prominent but were confined very much to the ends of the cylinder, at least 95% of the everted cylinder being a right circular cylinder. Secondly, the everted outer radius of the cylinder was much smaller than the theory given here would predict and the everted inner radius was reduce to zero, something that we have shown above cannot happen, at least for Varga, Blatz–Ko and exact materials, see Sections 2.1, 2.2 and 2.3. This would seem to suggest that the required reduction in outer everted radius would be achieved if we had a more accurate constitutive model of the material. We have considered a wide range of strain–energy functions and this does not offer a solution. We recall that a highly compressible foam rubber is modelled by an "equivalent" homogeneous material, see Blatz and Ko (1962) for example. However, if we consider the behaviour of foam materials a little more closely we see that a compression of such a material requires, essentially, the bending of the matrix "walls" surrounding the voids in the overall material. This requires relatively little effort and so give a highly compressible material. However, to produce, say, a uniaxial extension of such a material we would require to rotate and then subject the matrix material to a uniaxial extension which would require a significantly greater effort. Hence a foam rubber material would be expected to behave differently in extension and compression. For many deformations this will not be important and the usual homogeneous model will give both qualitative and quantitative results. However, for the eversion of a cylindrical tube, the everted outer radius is in a state of azimuthal tension

while the inner everted outer radius is in a state of compression. If the material is actually stiffer in tension than the homogeneous model suggests then the outer everted radius would be smaller than that predicted by the homogeneous model, precisely the effect that we are looking for.

Materials that behave differently in tension and compression have been considered by Green and Mkrtichain (1977a). Such materials can be thought of as a combination of two homogeneous models, one for the material in a state of pure dilatation, one for pure compression, and two transversely isotropic materials, one when two principal stretches are greater than unity, one when two principal stretches are less than unity, with appropriate matching conditions. An explicit model of such a linear elastic material has been given by Green and Mkrtichain (1977b), but there are no models for finite elastic materials. We aim to consider the eversion of cylinders composed of such materials in a separate paper.

Acknowledgements—The work of A.O. was supported by an SERC earmarked award.

REFERENCES

Adeleke, S. A. (1983) On the problem of eversion for incompressible elastic materials. *Journal of Elasticity* **13,** 63–69.

Blatz, P. J. and Ko, W. L. (1962) Applications of finite elasticity theory to deformation of rubbery materials. *Transactions of the Society for Rheology* **6,** 223–251.

Carroll, M. M. (1988) Finite strain solutions in compressible elasticity. *Journal of Elasticity* **20,** 65–92.

Carroll, M. M. and Horgan, C. O. (1990) Finite strain solutions for a compressible elastic solid. *Quarterly Applied Mathematics* **48,** 767–780.

Chadwick, P. (1972) The existence and uniqueness of solutions of two problems in the Mooney–Rivlin theory for rubber. *Journal of Elasticity* **2,** 123–128.

Chadwick, P. and Haddon, E. W. (1972) Inflation-extension and eversion of a tube of incompressible isotropic elastic material. *Journal of the Institute of Mathematics Applications* **10,** 258–278.

Chung, D. T., Horgan, C. O. and Abeyaratne, R. (1986) The finite deformations of internally pressurized hollow cylinders and spheres for a class of compressible elastic materials. *International Journal of Solids and Structures* **22,** 1557–1570.

Green, A. E. and Mkrtichian, J. Z. (1977a) Elastic solids with different moduli in tension and compression. *Journal of Elasticity* **7,** 369–386.

Green, A. E. and Mkrtichian, J. Z. (1977b) Torsion and extension of a tube with different moduli in tension and compression. *Journal of the Institute Mathematics Applications* **20,** 221–226.

Haughton, D. M. (1987) Inflation of thick-walled compressible elastic spherical shells. *IMA Journal of Applied Mathematics* **39,** 259–272.

Haughton, D. M. and Ogden, R. W. (1979a) Bifurcation of inflated circular cylinders of elastic material under axial loading—I. Membrane theory for thin-walled tubes. *Journal of Mechanics and Physics of Solids* **27,** 179–212.

Haughton, D. M. and Ogden, R. W. (1979b) Bifurcation of inflated circular cylinders of elastic material under axial loading—II. Exact theory for thick-walled tubes. *Journal of Mechanics and Physics of Solids* **27,** 489–512.

Haughton, D. M. and Orr, A. (1995) On the eversion of incompressible elastic cylinders. *International Journal of Non-Linear Mechanics* **30,** 81–95.

Hill, J. M. (1993) Cylindrical and spherical inflation in compressible finite elasticity. *IMA Journal of Applied Mathematics* **50,** 195–201.

Lindsay, K. A. and Rooney, C. E. (1992) A note on Compound matrices. *Journal of Computational Physics* **133,** 472–477.

Ogden, R. W. (1972) Large deformation isotropic elasticity: on the correlation of theory and experiment for compressible rubberlike solids. *Proceedings of the Royal Society, London* **A328,** 567–583.

Rivlin, R. S. (1949) Large elastic deformations of isotropic materials. VI Further results in the theory of torsion, shear and flexure. *Philosophical Transactions of the Royal Society, London* **A242,** 173–195.

Truesdell, C. (1978) Some challenges offered to analysis by rational thermodynamics. In *Contemporary Developments in Continuum Mechanics and Partial Differential Equations*, eds De La Penha, G. M. and Medeiros, L. A., pp. 496–540. North-Holland, Amsterdam.

APPENDIX

In this appendix we describe the numerical methods that have been used to solve the incremental equations (36)–(38) with boundary conditions (39). The general method is outlined by Lindsay and Rooney (1992) where other references can be found.

Firstly, consider the general homogeneous problem of $2n$ first order ordinary differential equations written in vector form

$$\frac{\mathrm{d}\mathbf{y}}{\mathrm{d}x} = \mathbf{A}(x,\gamma)\mathbf{y}, \quad a \leqslant x \leqslant b, \tag{A.1}$$

where $\mathbf{y}$ is a $2n$-vector and $\mathbf{A}$ is a $2n \times 2n$ matrix depending on the independent variable x and a parameter γ. The homogeneous boundary conditions are evenly distributed between the two ends of the range and can be written

$$\mathbf{B}(x,\gamma)\mathbf{y} = \mathbf{0}, \quad x = a, \tag{A.2}$$

and

$$\mathbf{C}(x,\gamma)\mathbf{y} = \mathbf{0}, \quad x = b, \tag{A.3}$$

where both $\mathbf{B}$ and $\mathbf{C}$ are $n \times 2n$ matrices. The aim is to determine values of the parameter (eigenvalue) γ so that non-trivial solutions exist. This seems to be typical of the problems encountered in both fluids and solid mechanics, but other cases with an odd number of equations and or an uneven distribution of boundary conditions can be treated in a similar way. (In some respects an even distribution of boundary conditions over the two ends constitutes the worst possible case as it involves most work.)

We can always choose n linearly independent vectors $\mathbf{y}^{(i)}$, $i = 1, 2, \ldots, n$ that satisfy all n boundary conditions at $x = a$, say. The general solution to (A.1) can then be written

$$\mathbf{y} = \sum_{i=1}^{n} k_i \mathbf{y}^{(i)}, \tag{A.4}$$

for some constants $k_1, k_2, \ldots, k_n$.

We define $\mathbf{M}$ to be the $2n \times n$ matrix whose ith column is $\mathbf{y}^{(i)}$. We then have

$$\mathbf{y} = \mathbf{M}\mathbf{k}, \tag{A.5}$$

where $\mathbf{k}$ is the n-vector $(k_1, k_2, \ldots, k_n)^T$. For future use we note from (A.1) that

$$\frac{\mathrm{d}\mathbf{M}}{\mathrm{d}x} = \mathbf{A}\mathbf{M}. \tag{A.6}$$

Equations (A.1) can be numerically integrated using each of $\mathbf{y}^{(i)}(a)$, $(i = 1, 2, \ldots, n)$ in turn as initial conditions to produce solutions $\mathbf{y}^{(i)}(b)$. The remaining boundary conditions (A.3) then become

$$\mathbf{C}(b,\gamma)\sum_{i=1}^{n} k_i \mathbf{y}^{(i)}(b) = \mathbf{C}\mathbf{M}\mathbf{k} = 0, \quad x = b. \tag{A.7}$$

The condition for the existence of non-trivial solutions is

$$\det(\mathbf{C}\mathbf{M}) = 0. \tag{A.8}$$

If the above $n \times n$ determinant is evaluated directly then we have essentially the method described by Haughton and Ogden (1979b), which has been used successfully for many problems of this type in elasticity. However, this method has proved to be inadequate for many problems in fluid mechanics, in particular the Orr–Sommerfeld problem, and also for the elastic bifurcation problems considered in Haughton and Orr (1995) and in this paper.

The compound matrix method avoids the necessity of evaluating a determinant directly which is the source of numerical instabilities even for very small values of n. The Laplace expansion of $\det(\mathbf{C}\mathbf{M})$ gives

$$\det(\mathbf{C}\mathbf{M}) = \sum_{i=1}^{{}^{2n}\mathrm{C}_n} \psi_i \phi_i, \tag{A.9}$$

where ψ_i and ϕ_i are $n \times n$ minors of $\mathbf{C}$ and $\mathbf{M}$, respectively. The summation takes place over all possible $n \times n$ minors of $\mathbf{M}$ taking rows of $\mathbf{M}$ in ascending order. Given a ϕ_i, ψ_i takes the corresponding columns of $\mathbf{C}$. The compound matrix method takes the set $\{\phi_i, i = 1, \ldots {}^{2n}\mathrm{C}_n\}$ as new set of dependent variables. The differential equations satisfied by the n-vector $\boldsymbol{\phi}$ are determined directly. The derivative of each minor give n $n \times n$ determinants the jth determinant has its j row differentiated and all other rows are unaltered. The differentiated row can be expressed as a linear combination of the rows of $\mathbf{M}$ by using (A.6) and hence as a linear combination of elements of $\boldsymbol{\phi}$. The coefficients that are required in this linear combination come from the original coefficient matrix $\mathbf{A}$. The ${}^{2n}\mathrm{C}_n$ differential equations are augmented with initial conditions chosen to be consistent with the original boundary conditions at $x = a$. Since $\mathbf{M}$ has rank n at least one of the compound matrix variables must be non-zero at $x = a$. Having integrated the ${}^{2n}\mathrm{C}_n$ equations *once only* we have the value of $\boldsymbol{\phi}$ at $x = b$. The condition (A.9) can be expressed as some (often trivial) linear combination of components of $\boldsymbol{\phi}$ at $x = b$ with coefficients obtained from the matrix $\mathbf{C}$. The parameter γ is then chosen to ensure that this "target" condition is satisfied. Essentially we have replaced the evaluation of an $n \times n$ determinant and the solution of $2n$ first order ordinary differential equations n times with a single solution of ${}^{2n}\mathrm{C}_n$ first order ordinary differential equations. The timing of the two methods is comparable but, as we shall see the second method returns a much higher degree of accuracy.

We now show how the compound matrix method is applied to the incremental equations (36)–(38) with boundary conditions (39). First we choose

$$\mathbf{y} = (f, f'g, g', h, h')^T. \tag{A.10}$$

Equations (36)–(38) can then be written

$$\mathbf{y}' = \mathbf{A}\mathbf{y}$$

where the components of the matrix $\mathbf{A}$ have the form

$$\mathbf{A} = \begin{bmatrix} 0 & 1 & 0 & 0 & 0 & 0 \\ A_{21} & A_{22} & A_{23} & A_{24} & A_{25} & A_{26} \\ 0 & 0 & 0 & 1 & 0 & 0 \\ A_{41} & A_{42} & A_{43} & A_{44} & A_{45} & 0 \\ 0 & 0 & 0 & 0 & 0 & 1 \\ A_{61} & A_{62} & A_{63} & 0 & A_{65} & A_{66} \end{bmatrix}, \tag{A.11}$$

the non-zero components are obtained from (36)–(38). The boundary conditions (39) become $\mathbf{Cy} = 0$, $r = a, b$ where

$$\mathbf{C} = \begin{bmatrix} -m & 0 & -1 & r & 0 & 0 \\ \alpha & 0 & 0 & 0 & 0 & 1 \\ C_{31} & C_{32} & 0 & C_{34} & C_{35} & 0 \end{bmatrix}, \tag{A.12}$$

where the unspecified components can be read off from (39). Since this problem involves six equations with three boundary conditions at each end of the interval we shall require ${}^6C_3 = 20$ compound variables and we shall consequently have to solve a system of 20 equations. The compound variables ϕ_i can be defined and a shorthand notation introduced as follows;

$$\phi_1 = \begin{vmatrix} y_1^{(1)} & y_1^{(2)} & y_1^{(3)} \\ y_2^{(1)} & y_2^{(2)} & y_2^{(3)} \\ y_3^{(1)} & y_3^{(2)} & y_3^{(3)} \end{vmatrix} = (1,2,3),$$

$$\phi_2 = \begin{vmatrix} y_1^{(1)} & y_1^{(2)} & y_1^{(3)} \\ y_2^{(1)} & y_2^{(2)} & y_2^{(3)} \\ y_4^{(1)} & y_4^{(2)} & y_4^{(3)} \end{vmatrix} = (1,2,4), \tag{A.13}$$

and similarly,

$$\begin{aligned} &\phi_3 = (1,2,5), \quad \phi_4 = (1,2,6), \quad \phi_5 = (1,3,4), \quad \phi_6 = (1,3,5), \quad \phi_7 = (1,3,6), \\ &\phi_8 = (1,4,5), \quad \phi_9 = (1,4,6), \quad \phi_{10} = (1,5,6), \quad \phi_{11} = (2,3,4), \quad \phi_{12} = (2,3,5), \\ &\phi_{13} = (2,3,6), \quad \phi_{14} = (2,4,5), \quad \phi_{15} = (2,4,6), \quad \phi_{16} = (2,5,6), \quad \phi_{17} = (3,4,5), \\ &\phi_{18} = (3,4,6), \quad \phi_{19} = (3,5,6), \quad \phi_{20} = (4,5,6), \end{aligned}$$

where we just have to take permutation of the integers from 1–6 in groups of three.

The generation of the differential equations satisfied by $\boldsymbol{\phi}$ is a straightforward but lengthy process. Lindsay and Rooney (1992) have produced a utility that generates standard fortran code for the required equations given the matrix **A**. To illustrate the process,

$$\begin{aligned} \phi_1' &= \begin{vmatrix} y_1'^{(1)} & y_1'^{(2)} & y_1'^{(3)} \\ y_2^{(1)} & y_2^{(2)} & y_2^{(3)} \\ y_3^{(1)} & y_3^{(2)} & y_3^{(3)} \end{vmatrix} + \begin{vmatrix} y_1^{(1)} & y_1^{(2)} & y_1^{(3)} \\ y_2'^{(1)} & y_2'^{(2)} & y_2'^{(3)} \\ y_3^{(1)} & y_3^{(2)} & y_3^{(3)} \end{vmatrix} + \begin{vmatrix} y_1^{(1)} & y_1^{(2)} & y_1^{(3)} \\ y_2^{(1)} & y_2^{(2)} & y_2^{(3)} \\ y_3'^{(1)} & y_3'^{(2)} & y_3'^{(3)} \end{vmatrix} \\ &= \begin{vmatrix} y_2^{(1)} & y_2^{(2)} & y_2^{(3)} \\ y_2^{(1)} & y_2^{(2)} & y_2^{(3)} \\ y_3^{(1)} & y_3^{(2)} & y_3^{(3)} \end{vmatrix} + \begin{vmatrix} y_1^{(1)} & y_1^{(2)} & y_1^{(3)} \\ \sum_{i=1}^{6} A_{2i} y_i^{(1)} & \sum_{i=1}^{6} A_{2i} y_i^{(2)} & \sum_{i=1}^{6} A_{2i} y_i^{(3)} \\ y_3^{(1)} & y_3^{(2)} & y_3^{(3)} \end{vmatrix} + \begin{vmatrix} y_1^{(1)} & y_1^{(2)} & y_1^{(3)} \\ y_2^{(1)} & y_2^{(2)} & y_2^{(3)} \\ y_4^{(1)} & y_4^{(2)} & y_4^{(3)} \end{vmatrix}, \end{aligned}$$

having used (A.10) and (A.11). Hence,

$$\phi_1' = A_{22}\phi_1 - A_{24}\phi_5 - A_{25}\phi_6 - A_{26}\phi_7 + \phi_2.$$

The other equations are obtained in a similar way. The initial conditions are obtained directly from (39). Choosing y_1, y_3, and y_5 as free variables (other choices are possible but not every combination is consistent with (39)), we express all of the initial conditions in terms of $\phi_6 = (1,3,5)$. For example,

$$\phi_1(a) = \begin{vmatrix} y_1^{(1)}(a) & y_1^{(2)}(a) & y_1^{(3)}(a) \\ y_2^{(1)}(a) & y_2^{(2)}(a) & y_2^{(3)}(a) \\ y_3^{(1)}(a) & y_3^{(2)}(a) & y_3^{(3)}(a) \end{vmatrix}.$$

Using (A.3) with (A.12) to rewrite $y_2(a)$ in terms of $y_1(a)$, $y_3(a)$, $y_5(a)$ we have

$$\phi_1(a) = \begin{vmatrix} y_1^{(1)} & y_1^{(2)} & y_1^{(3)} \\ \delta y_1^{(1)} + \beta y_3^{(1)} + \gamma y_5^{(1)} & \delta y_1^{(2)} + \beta y_3^{(2)} + \gamma y_5^{(2)} & \delta y_1^{(3)} + \beta y_3^{(3)} + \gamma y_5^{(3)} \\ y_3^{(1)} & y_3^{(2)} & y_3^{(3)} \end{vmatrix} = -\gamma\phi_6(a),$$

where

$$\delta = -(C_{31} + mC_{34}/a)/C_{32}, \quad \beta = -\frac{C_{34}}{aC_{32}}, \quad \gamma = -\frac{C_{35}}{C_{32}}, \quad C_{32} \neq 0.$$

Similarly,

$$\phi_2(a) = \begin{vmatrix} y_1^{(1)}(a) & y_1^{(2)}(a) & y_1^{(3)}(a) \\ y_2^{(1)}(a) & y_2^{(2)}(a) & y_2^{(3)}(a) \\ y_4^{(1)}(a) & y_4^{(2)}(a) & y_4^{(3)}(a) \end{vmatrix},$$

which can be written

$$\phi_2(a) = \begin{vmatrix} y_1^{(1)} & y_1^{(2)} & y_1^{(3)} \\ \delta y_1^{(1)} + \beta y_3^{(1)} + \gamma y_5^{(1)} & \delta y_1^{(2)} + \beta y_3^{(2)} + \gamma y_5^{(2)} & \delta y_1^{(3)} + \beta y_3^{(3)} + \gamma y_5^{(3)} \\ my_1^{(1)}/a + y_3^{(1)}/a & my_1^{(2)}/a + y_3^{(2)}/a & my_1^{(3)}/a + y_3^{(3)}/a \end{vmatrix} = -\gamma\phi_6(a)/a,$$

having again used (A.12). The completed initial vector $\boldsymbol{\phi}(a)$ is

$$\boldsymbol{\phi}(a) = \phi_6(a)[-\gamma, -\gamma/a, \beta, 0, 0, 1, 0, 1/a, 0, 0, -\gamma m/a, \delta, \alpha\gamma, \delta/a - m\beta/a, \alpha\gamma/a, -\beta\alpha, -m/a, 0, -\alpha, -\alpha/a], \tag{A.14}$$

where $\phi_6(a) \neq 0$ is arbitrary.

Finally, the target condition is obtained by using the boundary conditions (A.12) at $r = b$. Using similar shorthand notation to that introduced in (A.13) we require

$$(my_1 + y_3 - ry_4, \alpha y_1 + y_6, C_{31}y_1 + C_{32}y_2 + C_{34}y_4 + C_{35}y_5) = 0, \quad r = b.$$

Expanding this determinant leaves us with the target condition

$$C_{31}(\phi_7 - r\phi_9) + C_{32}(\alpha\phi_1 - \alpha r\phi_2 - m\phi_4 + \phi_{13} - r\phi_{15}) + C_{35}(r\phi_{20} - \phi_{19} + \alpha r\phi_8 - m\phi_{10} - \alpha\phi_6) + C_{34}(-\alpha\phi_5 - m\phi_9 - \phi_{18}) = 0, \quad r = b. \tag{A.15}$$

The compound matrix method then consists of solving the system of 20 1st order equations

$$\boldsymbol{\phi}' = \hat{A}\boldsymbol{\phi}, \tag{A.16}$$

(say) where $\hat{A}$ is a known 20×20 matrix subject to initial conditions (A.14). The bifurcation parameter within the system is then adjusted until the target condition (A.15) is satisfied.

The accuracy of the method depends only on the accuracy obtained in the solution (A.16).